Effects of 3D Magnetic Perturbations on Toroidal Plasmas

J.D. Callen, University of Wisconsin, Madison, WI 53706-1609 USA, `callen@engr.wisc.edu`

Abstract. Small 3D magnetic perturbations have many interesting and useful effects on tokamak and quasi-symmetric stellarator plasmas. Plasma transport equations that include these effects, most notably on diamagnetic-level toroidal plasma rotation, have recently been developed. The 3D magnetic perturbations and their plasma effects can be classified according to their toroidal mode number n. Low n non-resonant fields induce a neoclassical toroidal viscosity (NTV) that damps toroidal rotation throughout the plasma toward an offset flow in the counter-current direction; recent tokamak experiments have generally confirmed and exploited these predictions by applying external low n non-resonant magnetic perturbations. Medium n toroidal field ripple produces similar effects plus possible ripple trapping NTV effects and direct ion losses in the edge. A low n (e.g., $n=1$) resonant field is mostly shielded by the toroidally rotating plasma at and inside the resonant (rational) surface; if it is large enough it can stop plasma rotation at the rational surface, facilitate magnetic reconnection there and lead to a growing locked mode, which often causes a plasma disruption. Externally applied 3D magnetic perturbations usually have many components; in the plasma their lowest n (e.g., $n=1$) externally resonant components can be amplified by kink-type plasma responses, particularly at high β. Low n plasma instabilities (e.g., NTMs, RWMs) cause additional 3D magnetic perturbations in tokamak plasmas; tearing modes can bifurcate the topology and form magnetic islands. Finally, multiple resonant magnetic perturbations (RMPs) can, if not shielded by plasma flow effects, cause local magnetic stochasticity and influence H-mode edge pedestal transport. These various effects of 3D magnetic perturbations can be used to directly modify plasma toroidal rotation and indirectly plasma transport, e.g., for reducing anomalous transport and ELM control. The present understanding and modeling of these various effects, and key open issues for development of a predictive capability of them for ITER are discussed.

1   Magnetic Field Representation

Tokamaks are two-dimensional (2D) axisymmetric magnetic systems to lowest order. But small 3D perturbations $\delta\mathbf{B}$ arise from externally applied fields and plasma instabilities. The $\mathbf{B}$ field magnitude in near-axisymmetric tokamaks can be written using the poloidal magnetic flux ψ (radial coordinate), straight-field-line poloidal angle θ and axisymmetric toroidal angle ζ as

$$|\mathbf{B}| = \underbrace{|\mathbf{B}_0(\psi,\theta)|}_{\text{2D axisymm.}} + \sum_{n,m}\underbrace{\delta B_n(\psi,m)\cos\left(m\theta - n\zeta - \varphi_{m,n}\right)}_{\text{low } m,n \text{ resonant, non-resonant}} + \underbrace{\delta B_N(\psi,\theta)\cos(N\zeta)}_{\text{medium } n, \text{ ripple}} + \cdots. \quad (1)$$

The 3D magnetic perturbations and their effects on toroidal plasmas can be classified by their toroidal mode number n: low n (1 to 5) resonant (with magnetic field line pitch, $q=m/n$) and non-resonant fields, medium n (mainly due to ripple from N toroidal field coils) and high n ($\cdots$, due to microturbulence). Fields in quasi-symmetric stellarators can be represented similarly. This theory-based overview paper concentrates on low and medium n perturbations. Plasma flows are discussed first. Then, key 3D theory elements and finally combined effects are discussed.

2   Plasma Toroidal Rotation And Transport Equations

Key equations: Plasma transport equations for density, temperature and flows in tokamak plasmas that include 3D magnetic perturbation effects, including on diamagnetic-level plasma flows, have recently been developed [1]. These developments build on the fluid moment approach to stellarator plasma transport in which flows within a magnetic surface are obtained first [2], before the self-consistent radial electric field and net cross-field "radial" transport fluxes are determined. But they go one step further by assuming the 3D magnetic perturbations are gyroradius small compared to the axisymmetric (or stellarator quasi-symmetric) magnetic field. Then, various constraints on plasma flows are obtained on successive time scales [1]: 1) Radial ion force balance is enforced by compressional Alfvén waves on the μs time scale, which yields

$$\mathbf{V}_i\cdot\boldsymbol{\nabla}\zeta = -\left(\frac{\partial\Phi_0}{\partial\psi} + \frac{1}{n_iq_i}\frac{\partial p_i}{\partial\psi}\right) + q\,\mathbf{V}_i\cdot\boldsymbol{\nabla}\theta \quad\Longrightarrow\quad V_t \simeq \frac{E_\rho}{B_p} - \frac{1}{n_iq_iB_p}\frac{dp_i}{d\rho} + \frac{B_t}{B_p}\,V_p. \quad (2)$$

Thus, on the transport time scale the plasma toroidal flow V_t is a combination of $\mathbf{E} \times \mathbf{B}$, ion diamagnetic and poloidal ion flows. Here, B_p, B_t are the axisymmetric poloidal, toroidal magnetic field components and ρ (units of m) is a toroidal-flux-based radial coordinate. 2) The poloidal flow V_p is damped to a primarily ion-temperature-gradient diamagnetic-type flow on the ion collision ($\sim$ ms) time scale plus possible microturbulence-induced effects specified in [1b,1c]. Finally, 3) toroidal torque densities $\boxed{T_\zeta \equiv \mathbf{e}_\zeta \cdot \mathbf{F}_{\text{orce}}}$ ($\mathbf{e}_\zeta \equiv R^2 \boldsymbol{\nabla}\zeta = R\,\hat{\mathbf{e}}_\zeta$ is covariant toroidal angular vector) induce radial particle fluxes $\boxed{\boldsymbol{\Gamma}\cdot\boldsymbol{\nabla}\psi = -\,T_\zeta/q_s}$. Setting their summed radial current to zero (for ambipolar transport) yields the transport equation for plasma toroidal angular momentum density $\boxed{L_t \equiv \sum_{\text{ions}} m_i n_i \langle R^2 \mathbf{V}_i \cdot \boldsymbol{\nabla}\zeta\rangle}$ which, neglecting magnetic flux transients, is [1]:

$$\underbrace{\frac{\partial L_t}{\partial t}}_{\text{inertia}} \simeq \underbrace{-\langle \mathbf{e}_\zeta\cdot\boldsymbol{\nabla}\cdot\overleftrightarrow{\boldsymbol{\pi}}_{i\parallel}^{\text{3D}}\rangle}_{\text{NTV from } \delta B} + \underbrace{\langle \mathbf{e}_\zeta\cdot\overline{\delta\mathbf{J}\times\delta\mathbf{B}}\rangle}_{\text{resonant FEs}} - \underbrace{\langle \mathbf{e}_\zeta\cdot\boldsymbol{\nabla}\cdot\overleftrightarrow{\boldsymbol{\pi}}_{i\perp}\rangle}_{\text{cl, neo, paleo}} - \underbrace{\frac{1}{V'}\frac{\partial}{\partial\rho}\left(V'\Pi_{i\rho\zeta}\right)}_{\text{Reynolds stress}} + \underbrace{\langle \mathbf{e}_\zeta\cdot\textstyle\sum_s \bar{\mathbf{S}}_{sm}\rangle}_{\text{mom. sources}}. \quad (3)$$

The L_t solution of this equation gives the flux surface average (FSA) total plasma toroidal rotation frequency $\boxed{\Omega_t(\rho,t) \equiv \langle\mathbf{V}\cdot\boldsymbol{\nabla}\zeta\rangle = L_t/(m_i n_i\langle R^2\rangle) \sim V_t/R}$. Using (2), this Ω_t determines the radial electric field that yields ambipolar radial density transport [1]: $\boxed{E_\rho \equiv -\,|\boldsymbol{\nabla}\rho|\,\partial\Phi_0/\partial\rho \simeq}$ $\boxed{|\boldsymbol{\nabla}\rho|\left[\Omega_t\,\psi' + (1/n_{i0}q_i)\,dp_i/d\rho - (c_p/q_i)\,dT_i/d\rho\right]}$. Here, $\psi' \equiv d\psi/d\rho \simeq B_p R$, $c_p \equiv k_i \sim 1.17$ in $\sqrt{\epsilon} \ll 1$ neoclassical theory, $V' \equiv \partial V/\partial\rho \sim \varrho$ and V is the volume of the $\rho \equiv \sqrt{\psi_t/\pi B_{t0}}$ surface.

Plasma torques: Terms on the right of (3) represent [1] (in order of appearance) toroidal torque effects due to: non-resonant low and medium n 3D fields that induce neoclassical toroidal viscosity (NTV); low n resonant "field errors" (FEs); collision-induced classical, neoclassical and paleoclassical perpendicular viscosities; Reynolds (and Maxwell [1]) stress due to high n microturbulence (see [3]); and "external" toroidal momentum inputs. Relevant L_t boundary conditions and their effects, and integral forms of (3) are discussed in [1d]. In this comprehensive plasma toroidal rotation equation, radial particle fluxes induced by plasma toroidal torques are not individually ambipolar; rather, only their sum is. The requirement of ambipolar transport determines the plasma toroidal rotation (radial electric field). Since in tokamaks the dominant torques are on the ion species, the radial electric field is usually determined mainly by ion particle fluxes; this is called the "ion root" [of $\sum_s q_s\Gamma_s\cdot\boldsymbol{\nabla}\psi = f(E_\rho) \to 0$] in stellarator transport theory. The net radial particle transport flux [1b] is the sum of the intrinsically ambipolar collision-induced particle fluxes (classical plus neoclassical and paleoclassical) and non-ambipolar fluxes evaluated at the ambipolarity-enforcing radial electric field E_ρ (toroidal rotation frequency Ω_t). The radial energy transport fluxes induced by the low and medium n 3D field perturbations tend to be negligible since they are order $\varrho_*^2 (B_t/B_p)^2$ smaller [1] than the usual axisymmetric collision- and microturbulence-induced energy transport fluxes (here, $\varrho_* \equiv \varrho_i/a \ll 1$).

3   Low n Non-resonant δB Torques (applied by external coils)

Collision-induced toroidal torque: Using (2), the neoclassical toroidal viscous (NTV) torque induced by a single n non-resonant 3D perturbation can be written in the generic form

$$-\langle\mathbf{e}_\zeta\cdot\boldsymbol{\nabla}\cdot\overleftrightarrow{\boldsymbol{\pi}}_{i\parallel}^{\text{3D}}\rangle \simeq -m_i n_i\,\mu_\parallel\left(\frac{\delta B_n}{B_0}\right)^2\langle R^2\rangle\,(\Omega_t - \Omega_*), \quad \Omega_* \simeq \frac{c_p+c_t}{q_i}\frac{dT_i}{d\psi_p} \sim \frac{1}{q_i R B_p}\frac{dT_i}{d\rho} < 0. \quad (4)$$

This ion NTV torque damps toroidal rotation throughout the plasma toward an "offset" toroidal plasma rotation frequency Ω_*, which is in the counter-current direction, at a rate $\mu_\parallel(\delta B_n/B_0)^2$. All the seminal calculations of 3D-induced radial particle fluxes and NTV torques induced by δB_n in many possible asymptotic collisionality regimes have been made by Shaing [4].

Radial fluxes, NTV: The non-ambipolar radial particle fluxes and resultant NTV torques can be understood in terms of the collisional effects on radial drift motions induced by non-resonant 3D fields [1a,4f]. Phenomenologically, the particle diffusion coefficient can be written

as $D \sim f_\Delta \, (\Delta\rho)^2/\Delta t$ in which f_Δ is the velocity space fraction of particles taking random radial steps $\Delta\rho$ at a rate $1/\Delta t$. The NTV damping frequency obtained from $q_i \langle \mathbf{\Gamma \cdot \nabla} \psi \rangle = -T_\zeta = \langle \mathbf{e}_\zeta \mathbf{\cdot \nabla \cdot} \overset{\leftrightarrow}{\pi}{}^{\mathrm{3D}}_\parallel \rangle$ is $\mu_\parallel (\delta B_n/B_0)^2 \sim (D_i/\varrho_i^2)(B_p/B_0)^2 = (D_i/v_{d0}^2)(v_{Ti}^2/R_0^2)$ in which $\varrho_i \equiv v_{Ti}/\omega_{ci}$ is the ion gyroradius, $\epsilon \equiv r/R_0 \ll 1$ is the inverse aspect ratio and $v_{d0} \equiv 2T_i/(q_i B_p R_0) = (B_0/B_p)v_{Ti}(\varrho_i/R_0)$ with $v_{Ti} \equiv \sqrt{2T_i/m_i}$ is the reference (2D) gradient-B ion radial drift velocity [1a,4] due to the toroidal curvature ($\simeq 1/R_0$) of the tokamak.

Scalings: Approximate dimensional forms of relevant ion drift orbit effects and the induced ion diffusivities D_i, NTV damping frequencies $\mu_\parallel$ and 3D offset frequency coefficients c_t are shown in Table 1. In 2D axisymmetric theory the centers of both electron and ion banana drift orbits remain on a flux surface. Thus, 2D neoclassical transport is ambipolar and causes no NTV torque [1b]. (In the fluid approach the 2D torque T_ζ vanishes because there is no variation of $|\mathbf{B}|$ with ζ to impede flow in the toroidal direction.) The 3D fields introduce radial drifts of the centers of trapped-ion banana orbits ("banana-drifts" [4a]) with drift velocity $\boxed{v_d^{\mathrm{3D}} \equiv n\,(\delta B_n/B_0)\,v_{d0}.}$ Only trapped particles are involved in banana-drift effects. In the key $1/\nu$ regime in Table 1 the radial excursions of the banana centers are limited by collisions. In the key $\sqrt{\nu}$ regime they are limited by boundary layer effects on barely trapped particles. (The $\sqrt{\nu}$ regime includes and supersedes [4c] the originally calculated ν regime [4b].) In Table 1 $\boxed{\omega_E \equiv \partial\Phi_0/\partial\psi \simeq -E_\rho/RB_p}$ is the $\mathbf{E \times B}$-induced toroidal precession drift frequency [4b]. (Order unity logarithmic factors are neglected here and in Fig. 1.) When $\omega_E \to 0$ radial "superbanana plateau" (sbp) drift excursions are limited by the reference (2D) gradient-B drift frequency $\omega_{d0} \equiv v_{d0}/R_0$. Ripple-trapping effects [4h] are discussed in the next section. Finally, 3D fields produce transit (and bounce, drift) resonances and induce plateau-like diffusion [4i], which is highlighted in [4j] and comprehensively evaluated in [4k]. This effect is analogous to transit-time-magnetic-pumping (TTMP) effects by RF waves; Eq. (40) in [4i] provides a simple estimate for rippled tokamaks.

Collisionality regimes: The applicable ν_i ranges for the typically most important $1/\nu$, $\sqrt{\nu}$ and superbanana-plateau 3D trapped-ion transport are illustrated schematically in Fig. 1. Also shown are those for the standard 2D axisymmetric (banana, plateau and Pfirsch-Schlüter), 3D plateau (TTMP) and very low collisionality 3D superbanana [4f] transport. Since the 3D contributions from trapped ($1/\nu$, $\sqrt{\nu}$ and sbp) and transit-resonant particles (TTMP) arise from different regions of velocity space, at a given ion collision frequency their effects are additive.

Table 1: Particle diffusivities and NTV damping rates induced by ion drift orbit effects.

Regime	f_Δ	$\Delta\rho$	$\dfrac{1}{\Delta t}$	$D_i \sim f_\Delta \dfrac{(\Delta\rho)^2}{\Delta t}$	$\mu_\parallel \sim D_i \dfrac{n^2 v_{Ti}^2/R_0^2}{(v_d^{\mathrm{3D}})^2}$	c_t
2D axisymmetric						
banana	$\sqrt{\epsilon}$	$\Delta\rho_b \sim \dfrac{q\,\varrho_i}{\sqrt{\epsilon}}$	$\dfrac{\nu_i}{\epsilon}$	$\nu_i \dfrac{q^2 \varrho_i^2}{\epsilon^{3/2}}$	0	$-$
3D trapped particles $[\nu_i < \epsilon^{3/2}\omega_{ti}]$						
$\dfrac{1}{\nu_i} < \dfrac{1}{\epsilon\,|n|\omega_E}$	$\sqrt{\epsilon}$	$v_d^{\mathrm{3D}}\Delta t$	$\dfrac{\nu_i}{\epsilon}$	$\sqrt{\epsilon}\,\dfrac{(v_d^{\mathrm{3D}})^2}{\nu_i/\epsilon}$	$\sqrt{\epsilon}\,\dfrac{n^2 v_{Ti}^2/R_0^2}{\nu_i/\epsilon}$	2.4
$\sqrt{\dfrac{\nu_i}{\epsilon\,|n\omega_E|}} < 1$	$\sqrt{\epsilon}\left(\dfrac{\nu_i/\epsilon}{|n\omega_E|}\right)^{1/2}$	$\dfrac{v_d^{\mathrm{3D}}}{|n\,\omega_E|}$	$|n\omega_E|$	$\sqrt{\dfrac{\nu_i}{|n\omega_E|}}\dfrac{(v_d^{\mathrm{3D}})^2}{|n\omega_E|}$	$\sqrt{\dfrac{\nu_i}{|n\omega_E|}}\dfrac{n^2 v_{Ti}^2/R_0^2}{|n\omega_E|}$	0.34
$\omega_E \to 0$ (sbp)	$\sqrt{\epsilon}\left(\dfrac{\nu_i/\epsilon}{|n|\omega_{d0}}\right)^{1/3}$	$v_d^{\mathrm{3D}}\Delta t$	$\left(\dfrac{\nu_i n^2 \omega_{d0}^2}{\epsilon}\right)^{1/3}$	$\sqrt{\epsilon}\,\dfrac{(v_d^{\mathrm{3D}})^2}{|n|\omega_{d0}}$	$\sqrt{\epsilon}\,\dfrac{n^2\,v_{Ti}^2/R_0^2}{|n|\,\omega_{d0}}$	0.0
ripple trapped	$\left(\dfrac{\delta B_N}{B_0}\right)^{1/2}$	$\dfrac{B_p}{B_0}v_{d0}\Delta t$	$\dfrac{\nu_i}{\delta B_N/B_0}$	$\left(\dfrac{\delta B_N}{B_0}\right)^{3/2}\dfrac{B_p^2}{B_0^2}\dfrac{v_{d0}^2}{\nu_i}$	$\dfrac{(B_p^2/B_0^2)(v_{Ti}^2/R_0^2)}{(\delta B_N/B_0)^{1/2}\,\nu_i}$	3.5
3D transit-resonant particles $[\omega_{d0}(\delta B_n/B_0)^{3/2} < \nu_i < \omega_{ti},\ \mathbf{TTMP}]$						
plateau	$\left(\dfrac{\nu_i R_0}{|n|v_{Ti}}\right)^{1/3}$	$v_d^{\mathrm{3D}}\Delta t$	$\left(\dfrac{\nu_i n^2 v_{Ti}^2}{R_0^2}\right)^{1/3}$	$\dfrac{(v_d^{\mathrm{3D}})^2}{|n|v_{Ti}/R_0}$	$|n|\,(v_{Ti}/R_0)$	-0.5
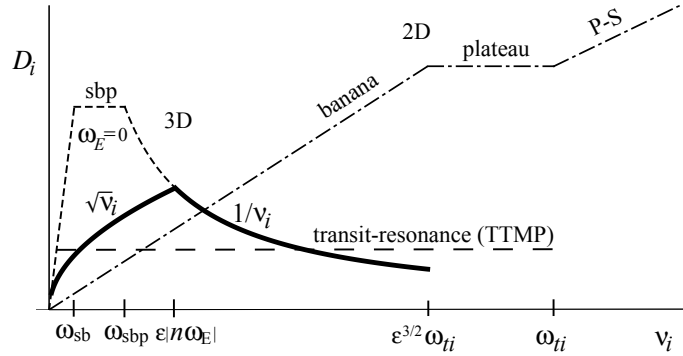
Figure 1: Ion collisionality regimes for 2D and 3D contributions to particle diffusivity $D_i \propto$ NTV damping frequency $\mu_\parallel$. Transitions occur at key frequencies: ion transit $\omega_{ti} \equiv v_{Ti}/R_0 q$, $\mathbf{E} \times \mathbf{B}$-induced $\epsilon |n \omega_E|$, superbanana-plateau radial drift $\omega_{\rm sbp} \equiv \epsilon |n| \omega_{d0}$ and superbanana $\omega_{\rm sb} \equiv \epsilon^{-1/2} (\delta B_n/B_0)^{3/2} (|n| \omega_{d0})$. The D_i and $\mu_\parallel$ become large when $\omega_E \rightarrow 0$ (short dashes curve).

Approximate multi-collisionality trapped-particle NTV torque formulas that include the radial force balance constraint and poloidal flow effects have recently been proposed [4e,f,g]. If ripple-trapping occurs, as discussed in the next section, its effects [4h] should also be added.

Initial experimental tests: Reduction of Ω_t induced by externally imposed non-resonant $(m/n = 1/3)$ 3D fields was first observed experimentally on DIII-D [5a] where it was compared to an adaptation of TTMP theory. Magnetic braking induced by TTMP effects of field errors was explored for JET plasmas [5b]. Reduction of the NTV damping rate with the degree of quasi-helical symmetry has also been demonstrated on HSX [5c]. Figures 2 and 3 show the first detailed comparisons of NTV theory (in the $1/\nu$ regime) with toroidal torque data from NSTX [5d]; this pioneering paper introduced the "neoclassical toroidal viscosity" (NTV) terminology. In retrospect, the good agreement shown in Figs. 2, 3 is a bit fortuitous — because later theory developments showed these NSTX plasmas were likely in the $\sqrt{\nu}$ regime where the NTV torque is somewhat smaller, but the competing "Lagrangian" effect [8c] of radial field line motion, which increases the $|\mathbf{B}|$ variations along field lines, was not included. Recent estimates of $n = 1$ NTV effects in JET [5e] found them to be too small; however the resonant field amplification (RFA) effects (see Section 6) found to be important in NSTX (see Fig. 3) were not included.

Experimental tests of offset: Damping of Ω_t by NTV to the offset frequency Ω_* in (4), which was first highlighted in [7f], has been convincingly demonstrated in DIII-D using a $n = 3$ non-resonant magnetic field (NMRF) [5f-h], as shown in Fig. 4. This paper introduced the
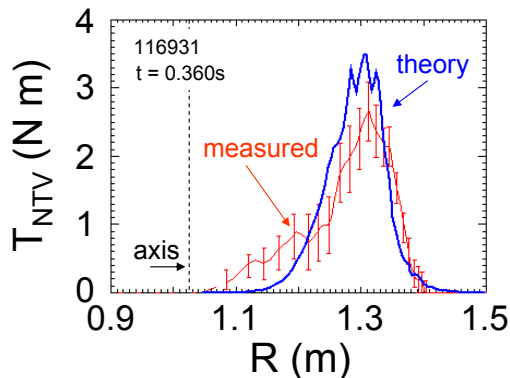
Figure 2: NSTX experimental test [5d] of the spatial profile and magnitude of NTV-induced torque $T_{\rm NTV}$ for $n = 3$ non-resonant 3D field.
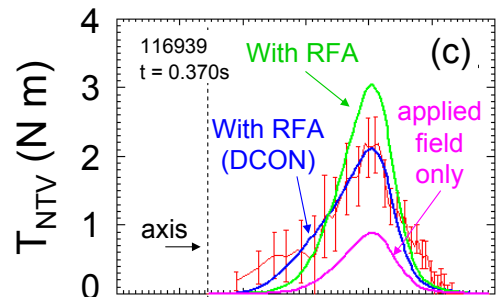
Figure 3: NSTX experimental test [5d] of the NTV torque shows resonant field amplification (RFA) effects are needed for $n = 1$ δB_n.
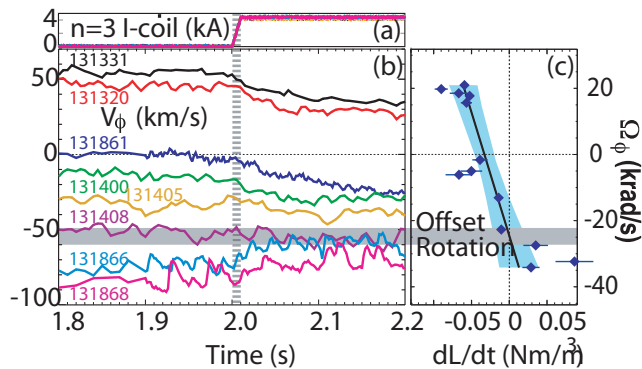
Figure 4: DIII-D experiments validated [5d,e] the NTV-induced damping/braking to offset rotation frequency Ω_* as implied by NTV formula in (4).
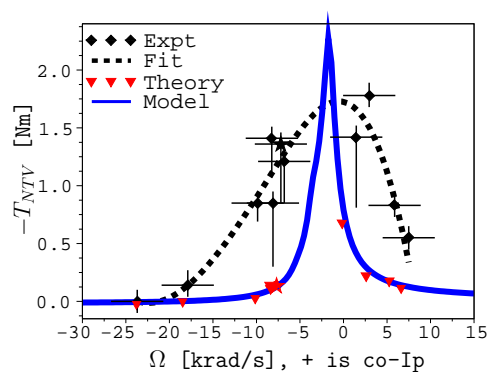
Figure 5: DIII-D experiments validated [5h] NTV peak caused by $\mu_\parallel(\nu_i, \omega_E)$ occurs where $\omega_E \simeq 0$ at which $\Omega_t \simeq -2$ krad/s.

"offset" rotation frequency terminology. The offset frequency Ω_* defined at the end of (4) is caused by superthermal ions diffusing radially more rapidly than thermal ions. Thus, a reduced toroidal rotation frequency Ω_t is required to obtain the same net torque and hence ambipolar radial particle transport compared to the case where T_i is spatially constant. Alternatively, from (2) the offset Ω_* represents the decrease in E_ρ needed to hold back more thermal ions to obtain ambipolar transport when $dT_i/d\rho < 0$. In addition, rotating MHD-type modes in MAST [5i] have been shown to induce torque and offset frequency effects consistent with NTV theory.

Peak NTV: The E_ρ-induced drift frequency $\boxed{\omega_E = -(1/n_i q_i)(dp_i/d\psi) + (c_p/q_i)dT_i/d\psi - \Omega_t}$ obtained from (2) varies with Ω_t. Thus, the NTV damping frequency $\mu_\parallel(\nu_i, \omega_E)$ and torque vary nonlinearly with Ω_t (ω_E). They peak where $\omega_E \to 0$, as indicated by the dashed curve in Fig. 1. This key effect has been demonstrated recently on DIII-D [5j], as shown in Fig. 5.

Status: Recent tokamak experiments have exploited NTV effects by applying $\delta B_n/B_0 \sim 10^{-3}$ low n non-resonant external magnetic perturbations to produce new regimes of QH-mode operation [5k] and reduce resonant field error effects [5l]. The composite of the various experimental tests and uses of the NTV torque validate to a large degree the neoclassical-based theory of the toroidal torque induced by the effects of externally applied low n non-resonant 3D fields.

4   Medium n Non-resonant δB Torques (toroidal field ripple)

Theoretical effects: The magnetic field ripple caused by the finite number N of toroidal field coils (typically $N = 18$–32, with $\delta B_N/B_0 \lesssim 10^{-2}$) induces various types of 3D NTV and direct ion loss effects, which are additive. The ripple-induced 3D trapped-particle contributions in Table 1 are usually in the $\sqrt{\nu}$ regime because $n \to N$ is large so typically $\nu_i < \epsilon |N\omega_E|$. The 3D transit-resonance (TTMP) effects [4i,j,k] can cause the dominant ripple effect. In addition, low collisionality ions with $\nu_i < (\delta B_N/B_0)^{1/2} N\omega_{ti}$ can be trapped in ripples (if $\epsilon |\sin\theta| < Nq\delta$ [4h]) causing ions to drift radially inducing a radial ion particle flux and hence NTV torque that scales as $(\delta B_n/B_0)^{3/2}$ [1a,4h], as indicated in the "ripple trapped" row of Table 1. Finally, near the plasma edge superthermal ions or NBI-produced fast ions can be ripple trapped or have up-down asymmetric banana drift orbits and drift out of the plasma. This "direct" FSA radial ion loss current $\langle \mathbf{J}_{dl} \cdot \nabla \psi_p \rangle$ induces a radial "return current" in the plasma to preserve quasineutrality [1b]. When this radially inward (negative) plasma return current is crossed with $\mathbf{B}_p$, it induces a toroidal torque on the edge plasma in the counter-current direction. This effect is represented in (3) by a momentum sink (see Section V of [1b]) $\langle \mathbf{e}_\zeta \cdot \bar{\mathbf{S}}_m \rangle = -\langle \mathbf{J}_{dl} \cdot \nabla \psi_p \rangle$. Thus, ripple-induced direct loss and NTV effects both decrease the plasma toroidal rotation frequency Ω_t; NTV effects damp it toward the offset rotation frequency Ω_* in the counter-current direction.

Experimental effects: A significant reduction in plasma toroidal rotation induced by ripple effects was first observed in ISX-B where adjacent toroidal field coils were de-energized
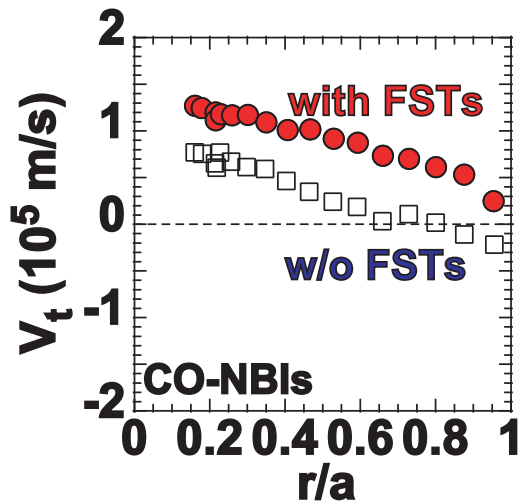
Figure 6: Toroidal plasma flow decreases as field ripple in JT-60U is increased from 1% (with FSTs) to 2% without (w/o) FSTs [6c].
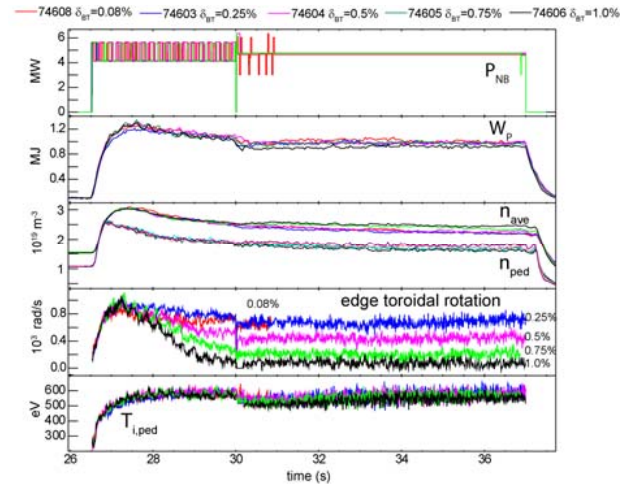
Figure 7: Toroidal plasma rotation decreases monotonically with increasing field ripple (% #s at right of 4th panel) in edge of JET [6e].

to produce an $N = 9$ coil system with an edge ripple of $\delta \equiv \delta B_N / B_0 \sim 10\%$ [6a]. Experiments in JT-60U L-mode plasmas with and without ferritic steel tiles (FSTs) to reduce the $N = 18$ field ripple (edge δ was reduced from 2% to 1%) observed a decrease in plasma toroidal flow toward the counter-current direction for the higher ripple case [6b], as shown in Fig. 6. This result agrees with theoretical modeling of the edge ripple-induced ion direct loss current effect [6c]. Also, the decrease in edge toroidal flow in JT-60U increases monotonically with increasing perpendicular NBI power which increases the edge direct ion loss current [6b]. Recently, variable-ripple experiments have been performed by changing the current in adjacent (even/odd) toroidal field coils. The edge ripple in the $N = 24$ JET configuration [6d,e,f] was varied from 0.08% to 1% and from 0.8% to 7% in Tore Supra experiments [6g]. The edge Ω_t decreased monotonically as ripple was increased [6d-g], as shown for JET in Fig. 7. All other plasma and pedestal profiles in JET were essentially unchanged as long as a ripple-induced "density pump-out" at the edge was compensated for by increased gas puffing to keep the overall plasma density constant [6e,h]. The differing ripple magnitudes between the JT-60U and full 24 coil JET experiments had previously been identified [6f] as the cause of slightly smaller pedestal pressures in JT-60U. Finally, analysis of the decrease in the edge Ω_t toward the counter-current direction in JT-60U has been shown [6i] to be proportional to $dT_i/d\rho$, which may be caused by the NTV Ω_* offset frequency.

Status: Decreases in edge Ω_t toward the counter-current direction caused by ripple-induced direct ion losses are in reasonable agreement with predictions [6c,j]. Modeling of ripple effects has concentrated on effects of the FSA direct ion loss current $\langle \mathbf{J}_{dl} \cdot \boldsymbol{\nabla} \psi_p \rangle$ and used phenomenological-type models [4a] for banana-drift effects [6c,6j] without taking account of self-consistent radial electric field effects (i.e., the Ω_t or ω_E dependence of the ripple-induced non-ambipolar ion radial particle fluxes). Modeling the full $\Omega_t(\rho)$ profile in rippled tokamaks when both NTV (from trapped and transit-resonant particles [4]) and edge ion direct loss effects are present requires self-consistent calculations using (3) and (4). Particularly important would be a modeling confirmation of the offset frequency Ω_* (< 0) effect in rippled tokamaks. Ripple-type effects caused by Test Blanket Modules (TBMs) being proposed for ITER are discussed in the final section.

5   Low n Resonant δB Torques (mode locking from field errors)

Locking physics: Field errors (FEs) often introduce low n resonant 3D magnetic perturbations; they can also be externally applied. Such 3D fields can induce "locked" (to the wall) MHD modes [7a,b] and lead to plasma disruptions. In ideal MHD an externally imposed 3D field induces a non-resonant $\delta\mathbf{B}$ response throughout the plasma but exerts no toroidal torque

on it [7c] — because there is no dissipation in the ideal MHD model. Dissipative nonideal (e.g., resistive) effects allow a resonant 3D field to induce a nonzero $\delta\mathbf{B}_{\rho\,m/n}$ in response to the induced ideal MHD delta-function "shielding current" $\delta\mathbf{J}_{\|m/n}$ within a thin "singular" layer of width δ_s around a low order rational surface defined by $q(\rho_{m/n}) = m/n$ [7c,d]. Nonideal effects produce a local Maxwell-stress-induced FSA toroidal torque density on the plasma for a cylindrical model in the form (representing the thin resistive singular layer at $\rho_{m/n}$ with a δ-function)

$$\langle \mathbf{e}_\zeta \cdot \overline{\delta\mathbf{J}_{\|m/n} \times \delta\mathbf{B}_{\rho\,m/n}} \rangle \simeq - m_i n_i \, (4nc_A^2) \left(\frac{\delta B_{\rho\,m/n}^{\rm vac}}{B_0} \right)^2 \left[\frac{(-\omega\tau_s)}{(-\Delta')^2 + (-\omega\tau_s)^2} \right] \frac{V\,\delta(\rho - \rho_{m/n})}{V'}. \quad (5)$$

Here, $c_A \equiv B_0/\sqrt{\mu_0 m_i n_i}$ is the Alfvén frequency, $\delta B_{\rho\,m/n}^{\rm vac} \equiv [\delta\mathbf{B}\cdot\boldsymbol{\nabla}\rho]_{\rho_{m/n}}$ is the radial component of the vacuum $\delta\mathbf{B}$ at $\rho_{m/n}$, $\omega \equiv \mathbf{k}\cdot\mathbf{V}_i = -n\Omega_t + m\langle\mathbf{V}_i\cdot\boldsymbol{\nabla}\theta\rangle = n\left[\omega_E + (1/n_i q_i)(dp_i/d\psi)\right]$, $\tau_s = \delta_s \rho_{m/n}/(\eta/\mu_0) \sim 10^2$–$10^{-3}$ s is the resistivity-induced singular-layer diffusion time, and Δ' is the tearing mode instability index (< 0 for stability). This radially localized torque density tries to stop plasma toroidal rotation at the rational surface induced by the momentum source $\langle\mathbf{e}_\zeta\cdot\sum_s\mathbf{S}_{sm}\rangle$. However, radial diffusion of the toroidal flow by the collision- and microturbulence-induced perpendicular viscous diffusivity $\chi_{\zeta i}$ limits the change in Ω_t in the vicinity of the singular layer. The ω (and hence Ω_t-, ω_E-dependent) factor in square brackets in (5) represents the nonideal (resistive) singular layer effects; its $\omega/(\omega^2 + \omega_0^2)$ dependence causes the plasma response to be analogous to induction motor responses to a rotating magnetic field [7c,d]. For $|\omega\tau_s| \gg 1$ plasma toroidal rotation and $\chi_{\zeta i}$ inhibit penetration of $\delta B_{\rho\,m/n}$ into the singular layer by producing an ideal MHD-type "superconducting plasma" shielding response for $\rho \leq \rho_{m/n}$ [7b-d]; i.e., in a cylindrical model it causes $\delta B_{\rho\,m/n}^{\rm vac}$ to vanish for $\rho \leq \rho_{m/n}$. However, when $\delta B_{\rho\,m/n}^{\rm vac}$ is large enough to reduce $|\omega\tau_s|$ to about $-\Delta' \sim 2m$, the "penetration threshold" is exceeded (e.g., for $\delta B_{\rho\,2/1}^{\rm vac}/B_0 \gtrsim 10^{-4}$ [7]), $\Omega_t(\rho_{m/n})$ is no longer restrained by $\chi_{\zeta i}$ effects and plasma rotation no longer "shields" out the resonant torque. Then, the solution of (3) bifurcates (in a few ms) to a state where the toroidal rotation vanishes at the rational surface, magnetic reconnection occurs at $\rho_{m/n}$ and a growing m/n locked mode magnetic island is induced, which often leads to a plasma disruption.

Recent theory developments: More physically relevant (mainly Visco-Resistive regime) two-fluid singular layer effects have recently been developed [7e]. In addition, NTV adds a global torque effect that attempts to keep the plasma rotating at the rate Ω_* [7f]; it amplifies the viscosity-induced plasma rotation shielding effects by a factor $\Gamma_s \equiv [\rho_{m/n}^2 \mu_\| (\delta B_{\rho\,m/n}^{\rm vac}/B_0)^2/\chi_{\zeta i}]^{1/2}$ when it exceeds unity. Finally, and perhaps most critically for mode-locking thresholds at fusion-relevant β values, resonant field amplification (RFA) mainly due to weakly damped kink-type $n=1$ resonant plasma responses [8] are being explored; they are discussed in the next section.

Recent experimental studies, status: Field error locking results from many tokamaks are summarized empirically in [7g], as shown in Fig. 8. The field error mode-locking threshold scales primarily about linearly with plasma density in ohmic-level plasmas. The recent NTV-influenced mode-locking theory [7f] agrees most closely with this scaling. However, detailed quantitative comparisons with theory require knowledge of the magnitude and scaling of the perpendicular ion momentum diffusivity $\chi_{\zeta i}$ and remain to be made. Recent detailed experimental studies of field error mode-locking thresholds obtained with a mix of intrinsic field errors and external fields applied to compensate them found plasma response effects [5c,e;8a] must be included [7h-k]; i.e., the torque in (5) depends on the plasma-response resonant $\delta B_{\rho\,m/n}^{\rm plasma}$ instead of just the vacuum field resonant field component there. The resonant field amplification (RFA) scales approximately linearly with β at high β [7i,j]; see the example in Fig. 9. Hence "dynamic" field error compensation is usually needed for optimum error field control as β increases [7k]. Also, non-resonant NTV is being used to control and compensate for field error effects on Ω_t [5j;7k]. Finally, phased ECCD and NTV have been used to get locked modes to "commit suicide" and not lead to plasma disruptions [7l].
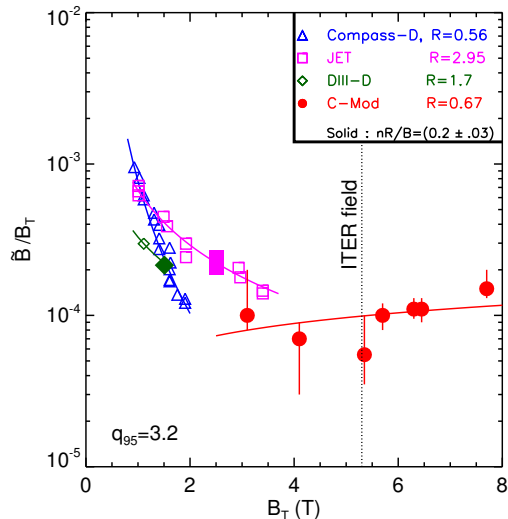
Figure 8: Relative threshold 2/1 magnetic perturbation ($\propto n_e R_0$ for solid points, $q_{95} \simeq 3.2$) above which locked modes occur [7g].
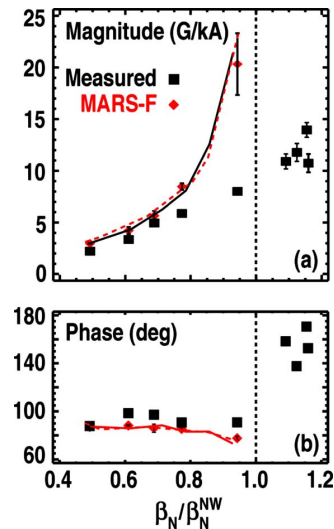
Figure 9: Magnitude of $n = 1$ 3D resonant field on DIII-D outer midplane increases $\propto \beta$ [7j]; ideal MHD MARS-F [8b] results shown.

6 Resonant Field Amplification (RFA) Plasma Responses To δB

Multiple Components: Externally applied 3D magnetic perturbations usually have many m, n Fourier components whose NTV, ripple-trapping and resonant FE effects should be summed in (3)–(5). However, the $\delta B_n(\psi, m)$ and $\delta B_{\rho\, m/n}$ amplitudes and phases $\varphi_{m,n}$ within the plasma need to be evaluated including plasma responses, i.e., not be vacuum values. Plasma responses to non-resonant fields are usually modest, except for β values near or above the no-wall limit [5c,e]. But for $n = 1$ resonant fields, Figs. 3 and 9 have already indicated the importance of plasma response effects for obtaining the correct magnitude of NTV and $\delta B_{\rho, m/n}$ effects.

Plasma Responses: Externally applied 3D fields can amplify resonant components of $\delta\mathbf{B}$ within the plasma if they couple to weakly damped MHD-type global eigenmodes in the plasma [8a,b]. The "least stable" (smallest damping rate) MHD-type eigenmodes are usually $n = 1$ kink-type modes that progressively "balloon" on the outboard side of the plasma cross section as β increases. Non-resonant fields don't naturally couple to $n = 1$ kink-type eigenmodes; thus, usually they are not significantly modified by plasma responses [8g]. However, externally applied 3D fields that can couple to the least stable $n = 1$ kink-type ideal MHD eigenmodes can amplify the $m/1$ magnetic field components within the plasma. Figure 10 shows the various m components of a representative kink-type $n = 1$ resistive wall mode (RWM) [7j]. Since at the plasma edge the dominant poloidal mode number m of a global $n = 1$ kink-type eigenmode is $m \gtrsim q \gtrsim q_{95}$, $m/1$ components of the externally applied $\delta\mathbf{B}$ that couple most strongly [7i,j] are those which are localized on the outboard midplane (where the straight-field-line θ coordinate values are most widely spaced) to $\Delta\theta \sim 2\pi/m$, as indicated in Fig. 11 [8c,d]. That is, $n = 1$ external field error (or error compensation) 3D components that cause the largest $\delta B_{\rho\, m/n}$ responses at the $m/n = 2/1, 3/1$ resonant surfaces within the plasma are those [7i,j] which are field-line-pitch-resonant with the external or edge $n = 1$ global kink eigenmode components with $m \gtrsim q \gtrsim q_{95}$ there.

Theory and modeling of plasma responses: The ideal MHD magnetic perturbation induced by a plasma displacement $\boldsymbol{\xi}$ is given by $\delta\mathbf{B} = \boldsymbol{\nabla}\times(\boldsymbol{\xi}\times\mathbf{B}_0)$; for finite $\boldsymbol{\xi}$ its radial component $\delta B_\rho \equiv \delta\mathbf{B}\cdot\boldsymbol{\nabla}\rho = (\mathbf{B}_0\cdot\boldsymbol{\nabla})(\boldsymbol{\xi}\cdot\boldsymbol{\nabla}\rho)$ must vanish at rational (resonant) surfaces in the plasma since $\mathbf{B}_0\cdot\boldsymbol{\nabla} \sim i(m - nq)/R_0 q$. In the ideal MHD model when an external 3D m/n resonant perturbation is applied to a rapidly rotating (i.e., $\omega\tau_s \gg 1$) plasma, a delta-function "shielding current" $\delta J_{\|\, m/n}$ must be introduced to satisfy this ideal MHD constraint [8a]. This generic procedure was used in the calculation of resonant field amplification (RFA)
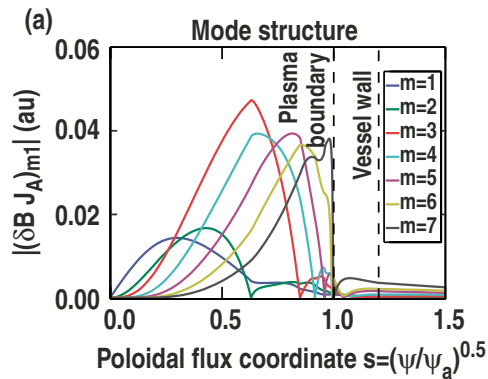
Figure 10: Poloidal mode spectrum of $\delta B_{\rho m/1}$ from nonideal MARS-F [8b] for an unstable RWM in DIII-D [7i] with $q_{95} \simeq 5$.
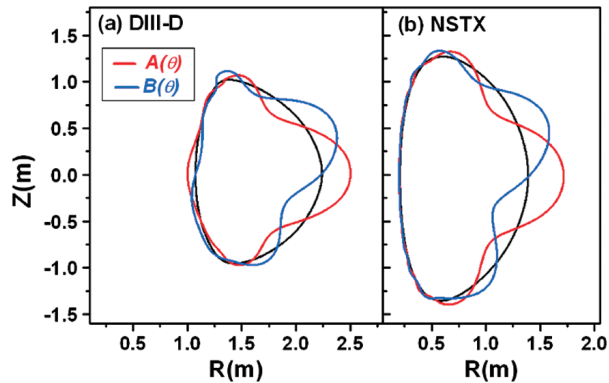
Figure 11: Distributions of external 3D fields from IPEC [8c] that maximize the total resonant fields on rational surfaces [8d] in a) DIII-D and b) NSTX.

effects in the original NTV explorations on NSTX [5c], as shown in Fig. 3. An innovative, comprehensive ideal perturbed equilibrium code (IPEC [8c]) has been developed to implement this procedure using the linear ideal MHD stability DCON code [8e]; it was used to produce the field error sensitivities shown in Fig. 11. The combination of the shielding current $\delta J_{\parallel m/n}$ and the (magnetically reconnected) $\delta B_{\rho,m/n}^{\mathrm{plasma}}$ this sheet current would produce if it were relaxed by resistivity or other non-ideal MHD effects has been used [8d] to estimate the resonant toroidal torque $\langle \mathbf{e}_\zeta \cdot \overline{\delta \mathbf{J}_{\parallel m/n} \times \delta \mathbf{B}_{\rho m/n}} \rangle$ by replacing the $\delta B_{\rho,m/n}^{\mathrm{vac}}$ in (5) with $\delta B_{\rho,m/n}^{\mathrm{plasma}}$ and using two-fluid layer physics [7e,f] for the term in square brackets in (5). This procedure provided encouraging explanations [8c] for field error correction effects in DIII-D and NSTX; however, while qualitative trends are captured, subsequent more precise evaluations have been less conclusive [8f]. Figure 9 shows that while the resonant field amplification (RFA) of $\delta B_{\rho m/n}$ increases about linearly with β well below the no-wall limit, the ideal MHD response (calculated in Fig. 9 with MARS-F) predicts too large a plasma response near (and beyond) the no-wall ideal MHD limit; non-ideal effects in the singular layer are critical for calculating the rotating plasma response and achieving stable plasmas above the no-wall limit, as in Fig. 10. The resonant toroidal torque $\langle \mathbf{e}_\zeta \cdot \overline{\delta \mathbf{J}_{\parallel m/n} \times \delta \mathbf{B}_{\rho m/n}} \rangle$ can be evaluated rigorously [8g] using a linear code such as MARS-F [8b]; when non-ideal MHD effects are included [8g,h], it can calculate self-consistently the singular layer effects and the reconnected resonant magnetic field $\delta B_{\rho m/n}^{\mathrm{plasma}}$ in the layer. More generally and comprehensively, nonlinear 3D initial value codes such as M3D [8i], NIMROD [8j] or reduced MHD codes (BOUT++ [8h] or JOREK [8k]) could calculate the resonant toroidal torque and also explore the dynamics of the field-error-induced mode locking process. To date these codes only use resistive MHD or limited two-fluid non-ideal MHD layer physics models; the neoclassical MHD inertia effects [8l,m] should also be included. Non-resonant 3D field components $\delta B_n(\psi, m)$ are also generated in response to edge-resonant $n = 1$ field error components and can cause NTV "global" toroidal flow damping effects in conjunction with resonant $\delta B_{\rho m/n}^{\mathrm{plasma}}$ effects [7i-k;8f].

Experimental studies, status: The first indications of plasma response effects were seen in 1992 in the β dependence of the mode locking thresholds in DIII-D [8n]. Resonant field amplification (RFA) was later observed above the no-wall β limit [8o,p] and shown to be caused a marginally stable $n = 1$ RWM [8p]. More recently, RWM-induced RFA proportional to β has been observed along with NTV damping effects in NSTX [8q]; e.g., see Fig. 9. The IPEC studies [8d,f] of plasma response effects induced by externally applied 3D fields to compensate for field errors were instrumental in demonstrating the importance of these effects. Understanding of plasma response effects and correction of both $n = 1$ and $n = 3$ intrinsic field errors have led to sustained high plasma toroidal rotation and record plasma durations free of MHD activity in NSTX [7k,5j]. The IPEC plasma response studies [8c,d,f] have also provided the impetus for

studies using MARS-F and nonlinear initial value codes of the plasma response effects including non-ideal MHD layer physics which are needed for more precise quantification of the non-ideal effects, particularly near and above the no-wall β limit and for the dynamics of mode-locking.

7 Low n Plasma-Instability-Induced δBs Plus 3D Field Effects

Direct effects: Classical and neoclassical tearing modes (NTMs) and resistive wall modes (RWMs) cause additional 3D magnetic perturbations in tokamak plasmas. Direct effects of these MHD-type instabilities are: 1) RWM-induced $\delta B_n(\psi, m)$ perturbations cause non-resonant low n NTV effects via (4); and 2) Resonant tearing modes bifurcate the magnetic topology and form magnetic islands within the plasma that complicate and modify NTV effects [4l].

RWMs: Above the no-wall β limit, low n (typically $n = 1, 2$) ideal MHD-type RWMs are stabilized if Ω_t is large enough for the resistive wall to represent a conducting wall to the rotating plasma. If the plasma is stationary, magnetic field perturbations penetrate the resistive wall and RWMs can become unstable. Very recent experiments have demonstrated that the minimum Ω_t is lower than previously thought [9a-c], apparently because of stabilizing kinetic-based effects [9d] due to thermal and fast ions [9a-c] whose toroidal precessional drifts resonate with the plasma rotation frequency ω. Even when RWMs are stabilized they increase RFA of the $n = 1$ $\delta\mathbf{B}$ in the plasma, as indicated in Fig. 9. This in turn increases the NTV damping of Ω_t, the sensitivity to low n field errors and the tendency for NTMs to be excited.

NTMs: For relevant β values the bootstrap current provides a source of free energy for tearing modes in addition to the usual current gradient source. Tearing modes can be nonlinearly excited by low m/n (typically 3/2 and 2/1) 3D magnetic perturbations or they can appear "spontaneously." The critical issue for both classical (Δ') and neoclassical (bootstrap current) tearing modes is: what is the threshold β_N for given combinations of $\delta B_{\rho m/n}$ and toroidal rotation. Recent experiments indicate that β_N thresholds become lower as Ω_t is reduced [10a]. When tearing modes occur they modify [4d,l] the radial ion flux and NTV torque in the vicinity of the island; then NTV effects become more complicated and larger [4l] with possible kinetic reductions due to reactive resonant Pfirsch-Schlüter current effects on the island width [10b].

8 Multiple Resonant Magnetic Perturbations (RMPs for ELMs)

Use of resonant magnetic perturbations (RMPs) [11a-c] to control ELMs is based on edge magnetic stochasticity [11d-f] to reduce pedestal region plasma gradients. Magnetic field stochasticity is caused by island overlap (Chirikov criterion). Key RMP effects are explained by this criterion, especially the q_{95} sensitivity and divertor flux patterns. But some effects may not be: electron heat transport is only slightly changed, but some density "pump-out" often occurs. Many possible RMP effects are currently being explored: 1) Most importantly, "screening" of RMP fields by Ω_t reduces the width of the stochastic region [11g-o]. 2) Density pump-out due to RMP-induced $\mathbf{E} \times \mathbf{B}$ cells [11g], large $\boldsymbol{\xi} \cdot \boldsymbol{\nabla}\rho$ near the X-point [11i,j], q_{95} resonances [11o] or turbulence [11p]; 3) Collision lengths comparable to the magnetic decorrelation length in the pedestal [11b]. 4) Possible "laminar" helical ribbons of magnetic flux in the pedestal, SOL regions [11q]. 5) Radial plasma current driven by combination of E_ρ and magnetic stochasticity [11r]. And 6) Kinetic simulation of RMP effects on the pedestal [11s]: screening of RMPs, reduced pedestal E_ρ key for density pump-out, and only untrapped particles contribute to Rechester-Rosenbluth transport. The precise mechanisms by which RMPs affect the pedestal and hence ELMs are still being clarified. However, RMP effects are stimulating interesting studies and developing tools for modifying edge plasma transport (particle, energy and Ω_t) and associated edge stability.

9 Effects Of Changes In Toroidal Rotation On Plasma Behavior

As the preceding discussion has indicated, 3D fields can directly affect plasma toroidal rotation via resonant field errors (for $\delta B_{\rho m/n}/B_0 \gtrsim 10^{-4}$), NTV (for $\delta B_n/B_0 \gtrsim 10^{-3}$) and toroidal field ripple (for $\delta B_N/B_0 \gtrsim 10^{-2}$). Sufficiently large resonant fields in the plasma cause its toroidal

rotation at the rational surface to lock to the wall $[\omega(\rho_{m/n}) \to 0]$ in a few ms; thereafter the rest of the $\Omega_t(\rho)$ profile relaxes slowly via the diffusive radial transport fluxes in (3). The NTV and ripple effects globally damp Ω_t toward an offset frequency $\Omega_* < 0$. Concomitant density and heat transport fluxes induced by 3D field effects are of order $\varrho_*^2 (B_t/B_p)^2$ smaller and hence usually negligible. Thus, theory predicts that 3D fields directly affect Ω_t but net ambipolar density and energy transport only indirectly — mainly through effects of changes in $\Omega_t(\rho)$ on microturbulence-induced n and T transport. Experimental results generally confirm this prediction in that they usually find that 3D fields can significantly affect Ω_t via field error, NTV and ripple effects but usually have much smaller (factors of 3 or greater) effects on n and T profiles. However, as the preceding section noted, sufficiently large RMPs can induce local magnetic stochasticity in the edge plasma and thereby increase n and T_e transport there.

10   Status, Open Issues (toward predictive capability for ITER)

TBMs: Recent experiments were performed [12] on DIII-D to explore possible effects of field errors introduced by ITER test blanket modules (TBMs, $\delta \equiv \delta B/B_0 \sim 1.2\%$). The TBM mock-up was toroidally localized ($\Delta\zeta \sim 2\pi/24$) with $\delta \sim 1$–3%. Its main effect was braking of Ω_t ($\propto \Omega_t$) with increasing δ, causing $\Delta\Omega_t/\Omega_t$ up to -50%. Changes in density, confinement and β were factors of $\gtrsim 3$ smaller. Mode locking sensitivity to the $n=1$ field was greater, especially for higher β and lower Ω_t; but it was easily compensated. A major issue for the previously described theory is that since the TBM is toroidally localized, it is represented by a very large δB_n Fourier spectrum ($\pm n$ up to $\gg 2\times24$ coils). NTV, FE and RFA theory needs to be developed for a delta-function toroidal field ripple. Nonetheless, 3D effects in the TBM test can be estimated by summing over all the Fourier δB_n coefficients. TBM test results were consistent with [12a] 3D effects theory, modeling. Global NTV Ω_t braking was semi-quantitatively predicted [13b] by IPEC [8c] calculations; the very small TBM-induced $n = 1$ edge field error is amplified in the core by edge coupling to a $n=1$ kink. The I-coil compensation of the TBM-induced $n=1$ field error was also semi-quantitatively matched [13b] by IPEC calculations. Finally, the TBM mainly affected Ω_t, with lesser effects on n, T transport (albeit with a slight density pump-out).

Status: As indicated in the preceding sections, the fundamental physics building blocks of NTV, ripple, field error and RFA effects of low and medium n 3D fields on plasma toroidal rotation are approaching predictive capabilities for present experiments. Studies of the "combined" effects of 3D fields on RWMs, NTMs and ELMs via RMPs are more in the developmental stage. ITER has a $N=18$ toroidal field system with relatively large ripple, even with FSTs ($\delta \lesssim 0.4\%$). Also, smaller toroidal torque densities will be induced in ITER by heating sources (e.g., NBI). Thus, the ripple-induced NTV toroidal torques will likely be dominant in (3). Hence, ITER plasmas will likely [5e,6d] rotate toroidally with a frequency near the diamagnetic-level $\Omega_* < 0$ in (4), i.e., in the counter-current direction. This lower, diamagnetic-level plasma toroidal rotation could produce some undesired effects: 1) greater sensitivity to $n = 1$ external 3D field errors and β that could induce locked modes?, 2) smaller radial electric field shear with less stabilization effects on microturbulence?, 3) reduced β_N thresholds for NTMs?, and 4) more reliance on kinetic ion effects to stabilize RWMs above the no-wall limit? Non-resonant fields in ITER may be able to use NTV effects to control $\Omega_t(\rho,t)$. Error field sensitivities in ITER have been estimated using the IPEC code [13]. Some additional important 3D field effects issues for ITER are: 1) precise 3D field characteristics required for stabilization or amelioration of ELMs, 2) density "pump-out" caused by FEs, RMPs and ripple, which is not yet understood, 3) RFA effects on $n=1$ fields in plasmas including two-fluid layer and low collisionality physics, and 4) determination of how small field errors must be to avoid locked modes as β is increased — and an assessment of the degree to which internal, dynamic FE compensation coils might be needed.

[1] **Transport equations:** a) J.D. Callen, A.J. Cole and C.C. Hegna, Nucl. Fus. **49**, 085021 (2009); b) Phys. Pl. **16**, 082504 (2009); c) J.D. Callen, C.C. Hegna and A.J. Cole, Phys. Pl. **17**, 056113 (2010); d) V.D. Pustovitov, THS/P4-02, 2010 Daejeon IAEA FEC.

[2] **Stellarators:** K.C. Shaing and J.D. Callen, Phys. Fl. **26**, 3315 (1983) and references cited therein.

[3] **High n microturbulence effects on toroidal flow:** a) P.H. Diamond et al., Nucl. Fus. **49**, 045002 (2009); b) A.G. Peeters et al., OV/5-4, 2010 Daejeon IAEA FEC.

[4] **NTV theory:** a) R.J. Goldston et al., Phys. Rev. Lett. **47**, 647 (1981); b) K.C. Shaing, Phys. Pl. **10**, 1443 (2003); c) K.C. Shaing et al., Phys. Pl. **15**, 082506 (2008); d) K.C. Shaing et al., Pl. Phys. Cont. Fus. **51**, 035009 (2009); e) A.J. Cole et al., UW-CPTC 08-8, June 2009; f) K.C. Shaing et al., Nucl. Fus. **50**, 025022 (2010); g) A.J. Cole et al., UW-CPTC 10-7, Nov. 2010; h) K.C. Shaing and J.D. Callen, Nucl. Fus. **22**, 1061 (1982); i) K.C. Shaing et al., Phys. Fl. **29**, 521 (1986); j) J-K. Park et al., Phys. Rev. Lett. **102**, 065002 (2009), Phys. Pl. **16**, 056115 (2009); k) K.C. Shaing et al., Pl. Phys. Cont. Fus. **51**, 075015 (2009); l) K.C. Shaing et al., THS/P5-13, 2010 Daejeon IAEA FEC.

[5] **NTV experiments:** a) R.J. La Haye et al., Phys. Pl. **9**, 2051 (2002); b) E. Lazzaro et al., Phys. Pl. **9**, 3906 (2002); c) S.P. Gerhardt et al., Phys. Rev. Lett. **94**, 015002 (2005), Phys. Pl. **12**, 056116 (2007); d) W. Zhu, S.A. Sabbagh et al., Phys. Rev. Lett. **96**, 225002 (2006); e) Y. Sun et al., EXS/P3-06, 2010 Daejeon IAEA FEC; f) A.M. Garofalo et al., Phys. Rev. Lett. **101**, 195005 (2008); g) A.M. Garofalo et al., Phys. Pl. **16**, 056119 (2009); h) W.M. Solomon et al., Nucl. Fus. **49**, 085005 (2009); i) M-D. Hua, I.T. Chapman et al., Pl. Phys. Cont. Fus. **52**, 035009 (2010); j) A.J. Cole et al., UW-CPTC 10-1, July, 2010 (submitted to Phys. Rev. Lett.); k) A.M. Garofalo et al., EXS/1-2, 2010 Daejeon IAEA FEC; l) S.P. Gerhardt et al., Pl. Phys. Cont. Fus. **52**, 104003 (2010). See also [7i;8q;9c].

[6] **Ripple Experiments:** a) S.D. Scott et al., Nucl. Fus. **25**, 359 (1985); b) M. Yoshida et al., Pl. Phys. Cont. Fus. **48**, 1673 (2006); c) M. Honda et al., Nucl. Fus. **48**, 085003 (2009); d) P.C. de Vries et al., Nucl. Fus. **48**, 035007 (2008); e) G. Saibene et al., Paper EX/2-1, 2008 Geneva IAEA FEC; f) G. Saibene et al., Nucl. Fus. **47**, 969 (2007); g) C. Fenzi et al., EXC/3-4, 2010 Deajeon IAEA FEC; h) H. Urano et al., EXC/P8-17; i) M. Yoshida et al., EX/3-2; j) A. Salmi et al., Contrib. Plasma Phys. **48**, 77 (2008).

[7] **Field Errors:** a) M.F.F. Nave, J.A. Wesson, Nucl. Fus. **30**, 2575 (1990); b) T.C. Hender et al., Nucl. Fus. **32**, 2091 (1992); c) R. Fitzptrick, Nucl. Fus. **33**, 1049 (1993); d) R. Fitzpatrick, "Driven Reconnection in Magnetic Fusion Experiments," (1995) from `http://farside.ph.utexas.edu/papers/lecture.html`; e) A. Cole and R. Fitzpatrick, Phys. Pl. **13**, 032503 (2006); f) A.J. Cole et al., Phys. Rev. Lett. **99**, 065001 (2007), Phys. Pl. **15**, 056102 (2008), g) S.M. Wolfe et al., Phys. Pl. **12**, 056110 (2005); h) J.-K. Park et al., Phys. Rev. Lett. **99**, 195003 (2007); i) H. Reimerdes et al., Nucl. Fus. **49**, 115001 (2009); j) M.J. Lanctot, Phys. Pl. **17**, 030701 (2010); k) J.E. Menard et al., Nucl. Fus. **50**, 045008 (2010); l) F. Volpe et al. (to be published). See also [5l;8q].

[8] **Plasma Responses:** a) A.H. Boozer, Phys. Rev. Lett. **86**, 5059 (2001), A.H. Boozer and C. Nührenberg, Phys. Pl. **13**, 102501 (2006); b) Y.Q. Liu et al., Phys. Pl. **7**, 3681 (2000); c) J.-K. Park et al., Phys. Pl. **14**, 052110 (2007); d) J.-K. Phys. Rev. Lett. **99**, 195003 (2007); e) A.H. Glasser and M.S. Chance, Bull. Am. Phys. Soc. **42**, 1848 (1997); f) J.-K. Park et al., Phys. Pl. **16**, 056115 (2009); g) M.S. Chu et al., THS/P5-04, 2010 Daejeon IAEA FEC; h) Y.-Q. Liu et al., THS/P5-10; i) `http://w3.pppl.gov/m3d/index.php`; j) `https://nimrodteam.org`; k) G. Huysmans et al., Phys. Rev. Lett. **87**, 245002 (2001); l) J.D. Callen and K.C. Shaing, Phys. Fl. **28**, 1845 (1985) ; m) H.R. Wilson et al., Phys. Pl. **3**, 248 (1995); n) R.J. La Haye et al., Nucl. Fus. **32**, 2119 (1992); o) A.M. Garofalo et al., Phys. Pl. **9**, 1997 (2002); p) H. Reimerdes et al., Phys. Rev. Lett. **93**, 135002 (2004); q) S.A. Sabbagh et al., Nucl. Fus. **46**, 635 (2006). See also [5d,g;7h-k].

[9] **RWMs:** a) J.W. Berkery et al., Phys. Pl. **17**, 082504 (2010); b) H. Reimerdes et al., EXS/5-4, c) S.A. Sabbagh et al., EXS/5-5; d) B. Hu, R. Betti, Phys. Rev. Lett. **93**, 1005002 (2004). See also [7i-k;8o-q].

[10] **NTMs:** a) R.J. Buttery et al., EXS/P5-03, 2010 Daejeon IAEA FEC; b) C.C. Hegna et al., THS/4-1.

[11] **RMP Effects:** a) T.E. Evans et al., Nature Physics **2**, 419 (2006); b) M.E. Fenstermacher et al., Phys. Pl. **15**, 056122 (2008); c) M.E. Fenstermacher et al., ITR/P1-30, 2010 Daejeon IAEA FEC; d) T.E. Evans et al., J. Nucl. Mat. **145-147**, 812 (1987); e) A. Grosman, Pl. Phys. Cont. Fus. **41**, A185 (1999); f) Ph. Ghendrih et al., Nucl. Fus. **42**, 1221 (2002); g) V.A. Izzo and I. Joseph, Nucl. Fus. **48**, 115004 (2008); h) M.S. Chu et al., THS/P5-04; i) Y.Q. Liu et al., THS/P5-10; j) A. Kirk et al., EXD/8-2; k) H.R. Strauss et al., Nucl. Fus. **49**, 055025 (2009); l) M. Bécoulet et al., 2010 Dublin EPS meeting m) L. Sugiyama et al., THS/P3-04; n) Q. Yu and S. Günter, THS/P3-06; o) Y. Liang et al., EXS/P3-04; p) Z. Yan et al., EXC/P3-05; q) O. Schmitz et al., EXD/P3-30, Phys. Rev. Lett. **103**, 165005 (2009), Nucl. Fus. **48**, 024009 (2008); r) V. Rozhansky et al., THC/P3-06; s) C.S. Chang et al., THC/P4-04.

[12] **TBM Effects:** a) M.J. Schaffer et al., ITR/1-3; b) G.J. Kramer et al., EXW/P7-12.

[13] **ITER Field Errors:** a) J-K. Park et al., Nucl. Fus. **48**, 045006 (2008); b) EXS/P5-12.